[Regular Paper]

Development of Streamline-based Heat Transport Model for Thermal Oil-recovery Simulation

Usman and Norio ARIHARA*

Earth Science, Resources and Environmental Engineering, Graduate School of Science and Engineering,
Waseda University, 3-4-1 Ohkubo, Shinjuku-ku, Tokyo 169-8555, JAPAN

(Received June 1, 2004)

The streamline method was extended to thermal oil-recovery simulation by developing an appropriate heat transport model based on the streamline method for implemention into a thermal recovery simulator. The heat transport model consisted of convection from the flowing phases and diffusion terms of gravity, capillary force, and conduction. An operator splitting technique was applied to decouple the convective and diffusive parts for separate solution. The convective part, a non-linear one-dimensional hyperbolic equation, was solved by the implicit single-point upwind scheme along the streamlines. The diffusive part, a non-linear, mixed hyperbolic-parabolic equation modeling gravity, capillary force and conduction, was solved using finite-difference discretization over the three-dimensional grid. The pressures for defining streamlines were obtained by solving the fluid flow equations with a finite-difference Newton method considering the compressibility, depletion and capillary forces. Simulations of hot water-flooding in two-dimensional and three-dimensional heavy-oil reservoirs were conducted to verify the model. The simulation results were compared with those of a commercial thermal simulator, which demonstrated that the streamline approach is a viable alternative to conventional finite-difference methods for heat transport calculations within a thermal simulator.

Keywords

Heat transport, Streamline method, Operator splitting technique, Thermal simulator, Hot water flooding

1. Introduction

Fluid transport calculations based on streamlines have been used successfully for years to model two-phase incompressible flow simulations[1)~4)]. The pressures for defining the streamlines are obtained by assuming that the reservoir fluids and rock are incompressible and that flow is in the steady state, which yields a time-independent equation that can be solved to define the fixed pressure distribution. Streamline tracking is performed with the pressure field to advance saturations or compositions. In this approach, the changing pressure field and the movement of fluids are not tightly connected, which results in inaccuracies in the solution.

The streamline approach has recently been extended to various applications, such as compositional and black oil problems for updating the composition and saturation[5)~7)]. In those cases, a non-linear equation for the pressure is solved assuming unsteady-state flow but compressible fluids and rock, followed by solving the conservation equations in sequence or fully implicitly, *i.e.* the pressure and the saturation equations are solved together along each streamline. In this approach, most of the physical parameters that depend on the pressure changes are accounted for throughout the solution.

The major limitation of the streamline method is that applicability is restricted to convective problems only. In practice, the contribution of physical diffusion due to gravitational and capillary forces must be considered in modeling a reservoir undergoing a displacement process. The model including diffusion cannot be solved using one-dimensional (1D) streamlines. The operator splitting technique has been proposed to avoid this restriction[7)~9)]. The idea is to isolate the convective flow from the diffusion due to gravity for separate solution. The first part is calculated along the common streamline trajectories and the second part is determined by the direction of gravity.

Based on recent advances in streamline-based simulation techniques, we have extended the methods to the thermal oil-recovery simulation. Modeling thermal processes is difficult due to the many complex mechanisms, high degree of non-linearity, and requirements for appropriate thermodynamic formulation to account for the changes in properties with temperature and pressure. The present study approached the problem from

* To whom correspondence should be addressed.
* E-mail: arihara@waseda.jp

a different angle in the streamline framework. An operator splitting technique was applied to handle the heat diffusion due to gravity, capillary, and conduction effects, and the implicit method was used for solving the highly non-linear convective streamline and diffusive equations. A practical rule was introduced to select the time step for pressure updates to reduce the time-lag effects on the coefficients in the phase conservation equations.

A sequential thermal simulator, which solves the pressure and heat equations sequentially, was developed and tested for simulations of hot water-flooding in heavy-oil reservoirs. First we performed simulation with a two-dimensional (2D) heterogeneous reservoir to evaluate the main characteristics of the streamline method such as the number of streamlines, the grid refinement along the streamlines, and the time step size. Then we performed three-dimensional (3D) simulation to examine how the gravity mechanism affects the production performance. The solutions obtained using a commercial thermal simulator[10] were used to compare and validate the developed model.

2. Thermal Oil-recovery Model

This study formulated a three-phase thermal oil-recovery model. Although the numerical examples presented in the later section deal with two-phase (hot water and oil) flow, the derivation in this section is also valid for three-phase (liquid water, steam, and oil) flow. Following the previous thermal models[11),12)], fluid and heat flow were assumed to obey Darcy's law and Fourier's heat conduction equation, respectively. Additional assumptions are (1) the hydrocarbon component is insoluble in the water phase, (2) the water component is not allowed to dissolve in the oil phase, (3) relative permeability and capillary pressures are independent of temperature, (4) heat flow consists of convection and conduction only, and (5) heat flow to and from overburden and underburden does not occur. Therefore, the specific forms of the mass conservation equations for the water and oil components are

$$-\nabla\cdot(\rho_{\mathrm{w}}\mathbf{u}_{\mathrm{w}})+q_{\mathrm{w}}=\frac{\partial(\phi S_{\mathrm{w}}\rho_{\mathrm{w}})}{\partial t} \tag{1a}$$

$$-\nabla\cdot(\rho_{\mathrm{o}}\mathbf{u}_{\mathrm{o}})+q_{\mathrm{o}}=\frac{\partial(\phi S_{\mathrm{o}}\rho_{\mathrm{o}})}{\partial t} \tag{1b}$$

Equations (1a) and (1b) have identical form because each phase consists of only one component, and there is no inter-phase transportation of the components. The total energy conservation is given as

$$\begin{aligned}&-\nabla\cdot(\rho_{\mathrm{w}}H_{\mathrm{w}}\mathbf{u}_{\mathrm{w}}+\rho_{\mathrm{o}}H_{\mathrm{o}}\mathbf{u}_{\mathrm{o}})\\&\quad+\nabla\cdot(K_{\mathrm{h}}\nabla T)+q_{\mathrm{w}}H_{\mathrm{w}}^{\mathrm{w}}+q_{\mathrm{o}}H_{\mathrm{o}}^{\mathrm{w}}\\&=\frac{\partial}{\partial t}\left(\phi(S_{\mathrm{w}}\rho_{\mathrm{w}}H_{\mathrm{w}}+S_{\mathrm{o}}\rho_{\mathrm{o}}H_{\mathrm{o}})+(1-\phi)\rho_{\mathrm{r}}C_{\mathrm{r}}T\right)\end{aligned} \tag{2}$$

The flux velocity, $\mathbf{u}_\alpha$, is represented by Darcy's law as

$$\mathbf{u}_\alpha=\frac{kk_{\mathrm{r}\alpha}}{\mu_\alpha}(\nabla p_\alpha-\rho_\alpha\nabla D) \tag{3}$$

The mass flow rate, q_α, of the α phase from a layer k at wells is given by Peaceman's formulation[13] as

$$q_\alpha=\frac{2\pi\Delta z_{\mathrm{k}}}{\ln\dfrac{r_{e,\mathrm{k}}}{r_{\mathrm{w,k}}}+s_{\mathrm{k}}}\frac{kk_{\mathrm{r}\alpha}\rho_\alpha}{\mu_\alpha}\left(p_{\mathrm{k}}^{\mathrm{w}}-p_{\alpha\mathrm{k}}\right)\Big/(\Delta x\Delta y\Delta z_{\mathrm{k}}) \tag{4}$$

where $p_{\mathrm{k}}^{\mathrm{w}}$ is the pressure in the wellbore, $p_{\alpha\mathrm{k}}$ is the phase pressure in the gridblock, $r_{\mathrm{w,k}}$ denotes the wellbore radius, $r_{\mathrm{e,k}}$ is the equivalent radius, and s_k represents the skin factor.

In addition to the conservation equations, certain ancillary relationships must be specified to calculate the rock and fluid properties. The water-oil and oil-gas capillary pressures are assumed to be functions of phase saturation. Relative permeabilities to water and gas are dependent on the phase saturation. The porosity is taken to be a linear function of pressure as

$$\phi=\phi_{\mathrm{ref}}(1+c_{\mathrm{r}}(p-p_{\mathrm{ref}})) \tag{5}$$

The three-phase oil relative permeability is calculated using the modified Stone's Model II as

$$k_{\mathrm{ro}}=k_{\mathrm{rocw}}\left[\left(\frac{k_{\mathrm{row}}}{k_{\mathrm{rocw}}}+k_{\mathrm{rw}}\right)\left(\frac{k_{\mathrm{rog}}}{k_{\mathrm{rocw}}}+k_{\mathrm{rg}}\right)-k_{\mathrm{rw}}-k_{\mathrm{rg}}\right] \tag{6}$$

where $k_{\mathrm{rocw}}=k_{\mathrm{row}}(S_{\mathrm{w}}=S_{\mathrm{wc}})=k_{\mathrm{rog}}(S_{\mathrm{g}}=0)$.

The phase densities ρ_{w} and ρ_{o} are modeled by a correlation function of T and p as[10]

$$\begin{aligned}\rho_\alpha(p,T)=\rho_\alpha^{\mathrm{sc}}\cdot\exp\big[&c_\alpha(p-p_{\mathrm{sc}})\\&-a(T-T_{\mathrm{sc}})-0.5b\left(T^2-T_{\mathrm{sc}}^2\right)\big]\end{aligned} \tag{7}$$

where c_α is the compressibility, and a and b are the thermal expansion coefficients. The phase viscosity may be specified using the following correlation[10]

$$\mu_\alpha=a_{\mathrm{vis}}\cdot\exp(b_{\mathrm{vis}}/T) \tag{8}$$

T is in absolute degrees, whereas a_{vis} and b_{vis} are empirical parameters with values determined from two viscosity measurements at different temperatures. The enthalpies of the water, oil, and gas phases are calculated as follows[10]:

$$C_{\mathrm{g}}(T)=c_1+c_2T+c_3T^2+c_4T^3 \tag{9a}$$

$$H_{\mathrm{vap}}(T)=h_{\mathrm{vap}}(T_{\mathrm{cr}}-T)^{e_{\mathrm{vap}}} \tag{9b}$$

$$H_{\mathrm{g}}(T)=\int_{T_{\mathrm{ref}}}^{T}C_{\mathrm{g}}(T)\,\mathrm{d}T \tag{9c}$$

$$H_l(T)=H_{\mathrm{g}}(T)-H_{\mathrm{vap}}(T),\ l=\mathrm{w},\mathrm{o} \tag{9d}$$

Here, $C_{\mathrm{g}}(T)$ is the heat capacity of the gas phase expressed by correlation with coefficients c_1 to c_4, $H_{\mathrm{g}}(T)$ is the gas-phase enthalpy, $H_l(T)$ is the water- and oil-phase enthalpy, and $H_{\mathrm{vap}}(T)$ is the vaporization enthalpy expressed by the critical temperature T_{cr} and constants h_{vap} and e_{vap}. Suggested values of those parameters for selected components are given in Reference (10).

The corresponding boundary and initial conditions

for the system given in Eq. (1) are:

$$\mathbf{u}_\alpha(\mathbf{x},t)\cdot\mathbf{n}=0,\quad \mathbf{x}\in\partial\Omega \tag{10}$$

$$\begin{aligned} p(\mathbf{x},0)&=p^0(\mathbf{x}),\quad \mathbf{x}\in\Omega\\ S_\alpha(\mathbf{x},0)&=S_\alpha^0(\mathbf{x}),\quad \mathbf{x}\in\Omega\end{aligned} \tag{11}$$

where **n** is the outward unit vector normal to the boundary $\partial\Omega$ of the reservoir domain Ω, and p refers to the oil-phase pressure. The boundary and initial conditions associated with Eq. (2) are described later.

3. Sequential Thermal Simulator

The present sequential solution method for thermal oil-recovery simulation differs in several ways from the methods reported in the literature[14),15)]. The streamline method instead of the finite difference method was applied in the sequential step for solving the energy conservation equations within a time step. Equations (1) and (4) are solved simultaneously for pressure and saturation with a Newton finite difference formulation. After these equations are solved, new values for pressure and saturation are obtained at grid point $\mathbf{x}_i$ and the bottom hole pressure of the k-th zone. The obtained pressures are then used to define the streamlines. The algorithm proposed by Pollock[16)] is used to lace streamlines through individual cells. The heat convection is then calculated along the streamlines using an implicit single-point upwind scheme to update temperatures followed by diffusion term calculations on reservoir grids. A flow diagram of this simulator is shown in **Fig. 1**.

The main emphasis of this paper is the streamline approach for heat transport, so the solution method of mass transport is not discussed here. Aziz and Settari[17)] and Fanchi[18)] give more details about the solution methods for fluid transport.

4. Streamline Approach for Heat Transport

A hot-water displacement process was formulated to demonstrate the applicability of the streamline method for heat transport. The mathematical model and the solution procedure are illustrated in the following sections.

4. 1. Streamline Energy Equation

To derive the energy equation for streamlines, the total velocity was first defined as a sum of Eq. (3) for the oil and water phases,

$$\mathbf{u}_t=\frac{kk_{ro}}{\mu_o}(\nabla p_o-\rho_o\nabla D)-\frac{kk_{rw}}{\mu_w}(\nabla p_w-\rho_w\nabla D) \tag{12}$$

The oil- and water-phase pressures are related to the water-oil capillary pressure as

$$p_w=p_o-P_{cwo} \tag{13}$$

Using Eq. (13), Eq. (12) can be rearranged as

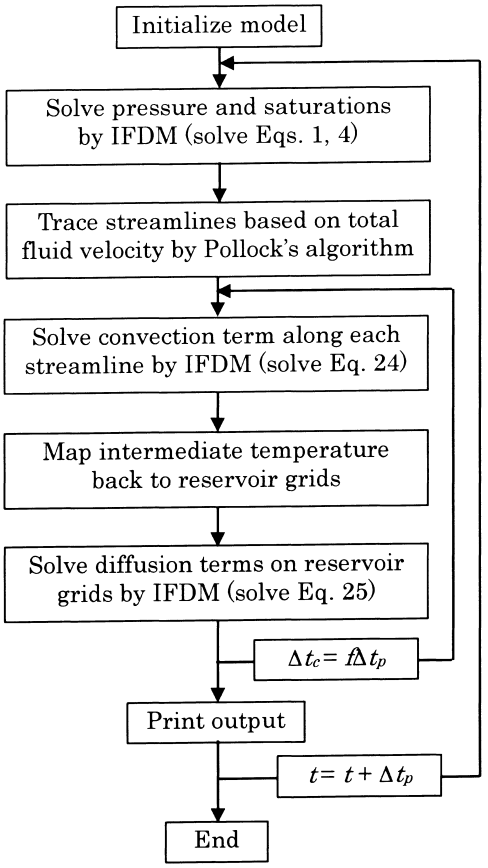

IFDM: implicit finite difference method.
f: specified fraction.

Fig. 1 Flow Chart for Streamline Simulation

$$\nabla p_o=-\frac{1}{\lambda_t}\left(\frac{\mathbf{u}_t}{k}-\lambda_w\nabla P_{cwo}-\lambda_w\rho_w\nabla D-\lambda_o\rho_o\nabla D\right) \tag{14}$$

where $\lambda_w=k_{rw}/\mu_w$, $\lambda_o=k_{ro}/\mu_o$, and $\lambda_t=\lambda_w+\lambda_o$. Inserting Eq. (3) into Eq. (2), and eliminating p_w and p_o by using Eqs. (13) and (14), the heat transport equation becomes,

$$\begin{aligned}&\frac{\partial}{\partial t}\left(S_w\rho_wH_w+S_o\rho_oH_o+\frac{1-\phi}{\phi}\rho_rC_rT\right)\\&+\frac{\mathbf{u}_t}{\phi}\cdot\nabla\left(f_w\rho_wH_w+f_o\rho_oH_o\right)\\&+\frac{1}{\phi}\nabla\cdot\left(k\gamma\nabla P_{cwo}\right)+\frac{1}{\phi}\nabla\cdot\mathbf{G}-\frac{1}{\phi}\nabla\cdot\left(K_h\nabla T\right)\\&=\frac{1}{\phi}\left(q_wH_w^w+q_oH_o^w\right)\end{aligned} \tag{15}$$

where

$$f_\alpha=\frac{\lambda_\alpha}{\lambda_t}=\frac{k_{r\alpha}/\mu_\alpha}{k_{rw}/\mu_w+k_{ro}/\mu_o},\ \alpha=w,o \tag{16}$$

$$\gamma=\frac{\lambda_w\lambda_o}{\lambda_t}\left(\rho_wH_w-\rho_oH_o\right) \tag{17}$$

$$\mathbf{G} = k\gamma(\rho_w - \rho_o)\nabla D \tag{18}$$

Since there is no obvious way to represent the term $\nabla\cdot\mathbf{u}_t$ along the streamline, we assumed $\nabla\cdot\mathbf{u}_t = 0$ when we derived Eq. (15).

The streamline method introduces the coordinate transformation for the convective term in Eq. (15). To do that, we defined the time-of-flight[16),19)], τ, along a streamline as

$$\tau(\mathbf{x}) = \int_0^s \frac{\phi}{|\mathbf{u}_t|} d\zeta \tag{19}$$

which leads to rewriting the operator as

$$\mathbf{u}_t \cdot \nabla = \phi \frac{\partial}{\partial \tau} \tag{20}$$

Using the above equation, Eq. (15) can be expressed as

$$\begin{aligned} &\frac{\partial E}{\partial t} + \frac{\partial F}{\partial \tau} + \frac{1}{\phi}\nabla\cdot(k\gamma\nabla P_{cwo}) \\ &+ \frac{1}{\phi}\nabla\cdot\mathbf{G} - \frac{1}{\phi}\nabla\cdot(K_h\nabla T) \\ &= \frac{1}{\phi}\left(q_w H_w^w + q_o H_o^w\right) \end{aligned} \tag{21}$$

Here, E is the total energy per unit volume written as

$$E = S_w\rho_w H_w + S_o\rho_o H_o + \frac{1-\phi}{\phi}\rho_r C_r T \tag{22}$$

and F is the energy convective flow defined as

$$F = f_w\rho_w H_w + f_o\rho_o H_o \tag{23}$$

The 3D convective problem is now transformed into the 1D problem to solve the energy equation, Eq. (21), along the streamlines.

4. 2. Streamline Operator Splitting

Equation (21) is recognized as a system of convection-diffusion equations with the diffusion term consisting of capillary, gravity, and conduction effects. As stated, the streamlines are less well suited to describe physical phenomena that transport fluid across the streamlines. In the streamline method, the fluid flow along each streamline is treated as independent, and the effects of the fluid flow transverse to the streamlines are not represented. However, physical diffusions can lead to flow transverse to the streamlines. By using the technique of operator splitting, we split these factors on a non-orthogonal grid, locally spanned by the streamlines and by the direction of diffusions. The advantage of decoupling the terms in Eq. (21) is that the diffusion can be solved independently and only solved in regions where they are important. Variations on this operator splitting approach have been taken by several authors[20)~22)].

Next we describe how to perform temperature calculations with the system given by Eq. (21) using an operator splitting method. Three steps are taken for calculating temperatures at the $n+1$ time step from the temperatures at the n time step.

Step 1: Let $T(\tau, t) = S_\zeta(t)T^n$ be the streamline solution to the convection part of Eq. (21) that is written as

$$\begin{aligned} &\frac{\partial E}{\partial t} + \frac{\partial F}{\partial \tau} = \frac{1}{\phi}\left(q_w H_w^w + q_o H_o^w\right); \\ &T(\tau, 0) = T^n(\tau); \quad T(0, \tau) = T_{inj}, t > 0 \end{aligned} \tag{24}$$

If $S_\zeta(t)$ denotes the operator that maps T^n to $T(\tau, t)$, we can define $T^{n+1/2} = S_\zeta(\Delta t)\, T^n$ as the intermediate solution, where subscript ζ stands for the grid spacing of the streamline solution.

Step 2: Let $T(\mathbf{x}, t) = R_\Delta(t)\, T^{n+1/2}$ be the finite difference solution to the diffusion parts of Eq. (21) that is written as

$$\begin{aligned} &\frac{\partial E}{\partial t} + \frac{1}{\phi}\nabla\cdot(k\nabla P_{cwo}\gamma) \\ &+ \frac{1}{\phi}\nabla\cdot\mathbf{G} - \frac{1}{\phi}\nabla\cdot(K_h\nabla T) = 0 \\ &T(\mathbf{x}, 0) = T^{n+1/2}(\mathbf{x}); \quad \nabla T(\mathbf{x}, t)\cdot\mathbf{n} = 0 \end{aligned} \tag{25}$$

Equation (25) is solved using N_d time steps of length k_d, *i.e.*, $k_d N_d = \Delta t$. The splitting solution at time t^{n+1} is given by $T^{n+1} = R_\Delta(\Delta t)T^{n+1/2}$, where the subscript Δ stands for the grid spacing of the finite difference solution.

Step 3: Then for a time $N\Delta t$, the approximated solution of Eq. (21) can be calculated with N-times repeated use of the operators as

$$T^{n+1}(\mathbf{x}) = [R_\Delta(\Delta t)\, S_\zeta(\Delta t)]\, T^n(\mathbf{x}) \tag{26}$$

4. 3. Numerical Solutions

We employed an implicit single-point upwind scheme along each streamline for Eq. (24) and implicit finite difference scheme for Eq. (25). Applying the implicit single-point upwind scheme for the convective streamline step has some striking advantages. First, the scheme requires no stability conditions, known as CFL (Courant-Fredrick-Lewy) conditions, associated with this method in the sense that time step, Δt, is not restricted by the spatial τ discretization parameter. Second, this scheme allows Eq. (24) to be solved on the irregularly spaced τ grid instead of the regular grid as when the equation is solved explicitly. On the other hand, the finite difference scheme to solve Eq. (25) slows the calculation because the capillary force and conduction must be solved in three dimensions, although the gravity equation can be solved over the gravity lines.

The implicit scheme for Eq. (24) requires calculations of the accumulation, E, the flux, F, and the fluid enthalpies, H_w^w and H_o^w, for each grid i at $k+1$ time level as

$$\frac{1}{\Delta t_c}\left[E\left(T_i^{k+1}\right)-E\left(T_i^{k}\right)\right]+\frac{1}{\Delta\tau}\left[F\left(T_i^{k+1}\right)-F\left(T_{i-1}^{k+1}\right)\right]-\frac{1}{\phi_i}\left[q_{wi}^{n+1}H_w^w\left(T_i^{k+1}\right)+q_{oi}^{n+1}H_o^w\left(T_i^{k+1}\right)\right]=0 \tag{27}$$

This is a non-linear equation for T_i^{k+1} which can be solved using Newton-Raphson's procedure[17),18)]. Equation (27) may be rewritten in terms of residual, R_c, which is equal to the left side of Eq. (27), as

$$R_c\left(T_i^{k+1}\right)=0 \tag{28}$$

The solution of Eq. (28) is obtained iteratively. For the first iteration ($v=1$), we use $T_i^v = T_i^k$, where T_i^k is known. Subsequent estimates for the updated temperatures are found as follows. First, we define the difference in temperature between two Newton iterations $v+1$ and v as

$$\delta T_i = T_i^{v+1} - T_i^v \tag{29}$$

δT_i at τ grid point i can be obtained by performing a Taylor series expansion of Eq. (28) with the first order in the small quantity δT,

$$R_{ci}^{v+1} = R_{ci}^v + \left(\frac{\partial R_{ci}}{\partial T_j}\right)^v \delta T_j \tag{30}$$

The value of δT_j that satisfies Eq. (28), $R_{ci}^{v+1}=0$, obeys the expression

$$\left(\frac{\partial R_{ci}}{\partial T_j}\right)^v \delta T_j = -R_{ci}^v \tag{31}$$

$\partial R_{ci}/\partial T_j$ is an element of the Jacobian matrix that is obtained numerically or analytically. Substituting Eq. (27) into Eq. (31) yields

$$\frac{1}{\Delta t_c}\left(\frac{\partial E}{\partial T}\right)_i^v \delta T_i + \frac{1}{\Delta\tau}\left[\left(\frac{\partial F}{\partial T}\right)_i^v \delta T_i - \left(\frac{\partial F}{\partial T}\right)_{i-1}^v \delta T_{i-1}\right] - \frac{1}{\phi_i}\left[q_{wi}^{n+1}\left(\frac{\partial H_w^w}{\partial T}\right)_i^v + q_{oi}^{n+1}\left(\frac{\partial H_o^w}{\partial T}\right)_i^v\right]\delta T_i = -R_{ci}^v \tag{32}$$

The solution is considered to converge when these increments of δT are smaller than the convergence criterion. The updated temperatures resulting from the solution of Eq. (32) have to be mapped back to the underlying grid in order to provide the initial condition, $T^{n+1/2}(\mathbf{x}) = T^{k+1}(\mathbf{x})$, for solving Eq. (25).

Following the procedure to derive Eq. (32), the discretized form of Eq. (25) is obtained in terms of the residual as

$$\begin{aligned}&\frac{V_b}{\Delta t_d}\left(\frac{\partial E}{\partial T}\right)_i^v \delta T_i + \Delta_x\left[\frac{k}{\phi}\left(\frac{\partial\gamma}{\partial T}\right)^v \Delta_x P_{cwo}^{n+1}\delta T\right]\\ &+\Delta_y\left[\frac{k}{\phi}\left(\frac{\partial\gamma}{\partial T}\right)^v \Delta_y P_{cwo}^{n+1}\delta T\right]\\ &+\Delta_z\left[\frac{k}{\phi}\left(\frac{\partial\gamma}{\partial T}\right)^v \Delta_z P_{cwo}^{n+1}\delta T\right]\\ &+\Delta_z\left[\frac{1}{\phi}\left(\frac{\partial G}{\partial T}\right)^v \delta T\right] - \Delta_x\left(\frac{K_h}{\phi}\Delta_x\delta T\right)\\ &-\Delta_y\left(\frac{K_h}{\phi}\Delta_y\delta T\right) - \Delta_z\left(\frac{K_h}{\phi}\Delta_z\delta T\right) = -R_{di}^v\end{aligned} \tag{33}$$

The solution of Eq. (33) gives the approximated solution of the system described by Eq. (21) at the $n+1$ time step for node i. The capillary term for x-direction is discretized as

$$\begin{aligned}&\Delta_x\left[\frac{k}{\phi}\left(\frac{\partial\gamma}{\partial T}\right)^v \Delta_x P_{cwo}^{n+1}\delta T\right]\\ &= TX_{Pci-1/2}\left(P_{cwo}\delta T\right)_{i-1}\\ &-\left(TX_{Pci-1/2}+TX_{Pci+1/2}\right)\left(P_{cwo}\delta T\right)_i\\ &+TX_{Pci+1/2}\left(P_{cwo}\delta T\right)_{i+1}\end{aligned} \tag{34}$$

Similarly, the discrete version of the conduction term for x-direction is

$$\begin{aligned}&\Delta_x\left(\frac{K_h}{\phi}\Delta_x\delta T\right) = TX_{Khi-1/2}\delta T_{i-1}\\ &-\left(TX_{Khi-1/2}+TX_{Khi+1/2}\right)\delta T_i + TX_{Khi+1/2}\delta T_{i+1}\end{aligned} \tag{35}$$

The coefficients in Eqs. (34) and (35) are given as follows:

$$\begin{aligned}TX_{Pci\pm1/2} &= \left(\frac{k}{\phi}\frac{\partial\gamma}{\partial T}\right)_{i\pm1/2}\frac{A_x}{\Delta x_{i\pm1/2}};\\ TX_{Khi\pm1/2} &= \left(\frac{K_h}{\phi}\right)_{i\pm1/2}\frac{A_x}{\Delta x_{i\pm1/2}}\end{aligned} \tag{36}$$

A difference approach is applied to the gravity term as

$$\begin{aligned}&\Delta_z\left[\frac{1}{\phi}\left(\frac{\partial G}{\partial T}\right)\delta T\right]\\ &= A_z\left[\frac{1}{\phi}\left(\frac{\partial G}{\partial T}\right)_{i+1/2} - \left(\frac{1}{\phi}\frac{\partial G}{\partial T}\right)_{i-1/2}\right]\delta T_i\end{aligned} \tag{37}$$

The upstream direction, at which G is to be evaluated, is dependent on the fluids, and is based on the flow direction[9)]. For the case of a two-phase water-oil system in which the oil is less dense than water, the proper approximation of $(\partial G/\partial T)_{i+1/2}$ is based on the water properties at node i and the oil properties at node $i+1$. A similar approach is employed for $(\partial G/\partial T)_{i-1/2}$.

In actual applications, the iterative calculations for Eqs. (32) and (33) tend to converge quickly. Our numerical experiments on hot water-flooding showed that the first approximation, T^{v+1}, is sufficiently accurate and that additional approximations are not warranted.

Table 1 Data for Simulation

Phase	Coefficients of viscosity calculations		Coefficients of enthalpy calculations					
	a_{vis} [Pa·day]	b_{vis} [K]	c_1	c_2	c_3	c_4	h_{vap}	e_{vap}
Oil	5.18E-13	5088.9	−22.38	1.939E+0	−1.117E-3	2.528E-7	287.1	0.625
Water	4.36E-11	1610.7	32.24	1.924E-3	1.055E-5	−3.596E-9	25.1	0.38

Phase	Critical properties			Coefficient of density calculations			
	M [kg/gmol]	T_{cr} [°C]	p_{cr} [kPa]	ρ^{sc} [kg/m^3]	c [kPa^{-1}]	a [°C^{-1}]	b [°C^{-2}]
Oil	0.600	493.8	1.118E+3	972	7.30E-7	3.80E-4	0.00E0
Water	0.018	374.1	2.206E+4	998	4.57E-7	−1.91E-3	0.00E0

Water-oil relative permeability			
S_w	k_{rw}	k_{rwo}	P_{cwo}
0.2175	0.0000	0.7200	0.0000
0.2464	0.0018	0.6142	0.0000
0.2636	0.0039	0.5635	0.0000
0.2976	0.0106	0.4667	0.0000
0.3306	0.0194	0.3760	0.0000
0.3645	0.0317	0.2923	0.0000
0.3989	0.0464	0.2161	0.0000
0.4319	0.0640	0.1479	0.0000
0.4659	0.0839	0.0890	0.0000
0.4828	0.0951	0.0637	0.0000
0.5159	0.1186	0.0223	0.0000
0.5328	0.1315	0.0079	0.0000
0.5500	0.1450	0.0000	0.0000
1.0000	0.2923	0.0000	0.0000

Gas-oil relative permeability			
S_l	k_{rg}	k_{rog}	P_{cog}
0.2175	0.0252	0.0000	0.0000
0.7715	0.0021	0.0000	0.0000
0.7878	0.0019	0.0001	0.0000
0.8041	0.0017	0.0011	0.0000
0.8205	0.0015	0.0034	0.0000
0.8531	0.0012	0.0153	0.0000
0.8858	0.0009	0.0409	0.0000
0.9021	0.0008	0.0604	0.0000
0.9184	0.0007	0.0851	0.0000
0.9347	0.0006	0.1157	0.0000
0.9511	0.0005	0.1527	0.0000
0.9674	0.0004	0.1969	0.0000
0.9837	0.0000	0.2417	0.0000
1.0000	0.0000	0.7200	0.0000

Rock thermal conductivity	[kJ/(m·sec·°C)]	3.5E-3
Reservoir heat capacity	[kJ/(m^3·°C)]	2347
Porosity at reference pressure		0.3
Reference pressure	[kPa]	6890
Reference temperature	[°C]	15.6
Surface pressure	[kPa]	100
Surface temperature	[°C]	15.6

The crucial point for the numerical solution is the selection of the time step size. There are two main time steps in this developed simulator: the time step elapsed between pressure updates, Eq. (1), and the time step used in the streamline energy equation, Eq. (21). As the temperature greatly affects the water and oil densities and viscosities involved in the coefficients of the pressure equation, the calculation of pressure updates is mainly controlled by the magnitude of the changes in temperature updates. When the maximum value of the temperature changes exceeds the specified constraint, a new pressure distribution is calculated. The time step for solving Eq. (21) depends on the numerical scheme and the physical parameters considered in the model. This issue remains for further studies, though typical values were found to be 0.2 to 1.0 times the pressure time step in the numerical experiments.

5. Model Performance

A sequential thermal oil-recovery simulator was developed implementing the streamline-based heat transport model. Simulations of hot water-flooding in heavy-oil reservoirs were conducted to examine the performance of the developed simulator. The simulation results were compared with the results of an existing commercial thermal simulator (CMG's STARS) to verify and evaluate the proposed methods.

5. 1. Problem Descriptions

The illustrative problem is a heavy oil reservoir of 14°API oil that underwent conventional (cold) water-flooding at the reservoir temperature. The modeled region of the reservoir is a quarter of the repeated five-spot pattern with an area of 75×75 m^2 and thickness of 5 m. The model includes two wells of 0.09 m wellbore radius, an injection well placed at the lower left

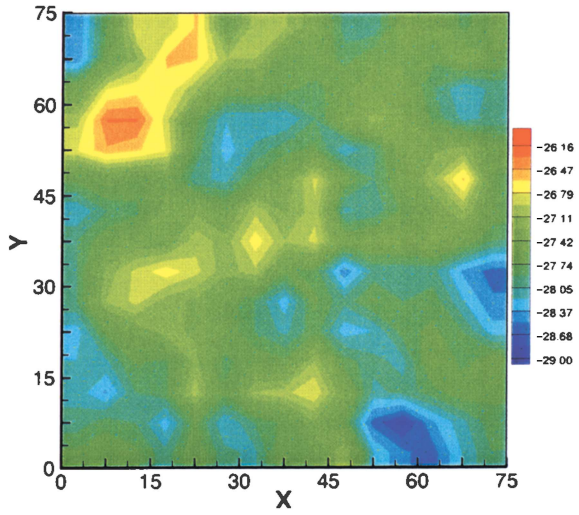

Fig. 2 Permeability Field Used for 2D Simulation

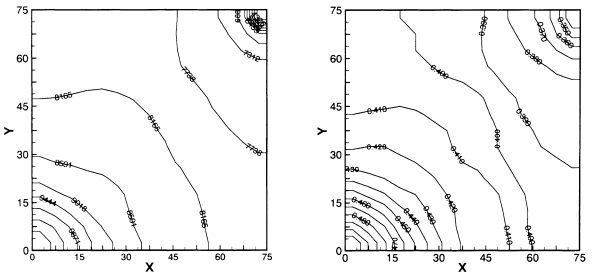

(a) Initial Oil Pressure (kPa) (b) Initial Water Saturation

Fig. 3 Initial Conditions of Pressure and Water Saturation for 2D Case, (a) Initial Oil Pressure (kPa), (b) Initial Water Saturation

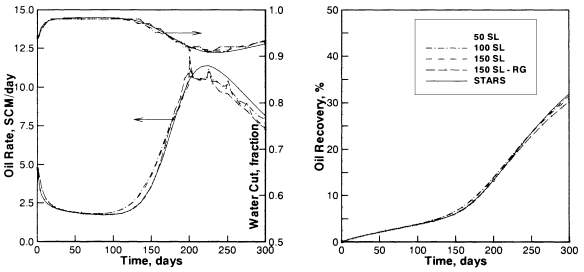

(a) Oil Rate and Water Cut (b) Oil Recovery

Fig. 4 Comparison of Production Performances of 2D Simulation, (a) Oil Rate and Water Cut, (b) Oil Recovery

edge of the region and a production well placed at the upper right edge. Fluid and rock properties, and the reservoir and surface conditions are listed in **Table 1**. Hot water of 150°C is injected at the constant rate of 100 m^3/day cold water equivalent. The producer well is operated under the minimum bottom-hole pressure constraint of 100 kPa. We ran the simulator for 300 days or the equivalent of 3.18 pore volume injected (PVI) with the constraints of the maximum changes in the basic variables allowed over a time step as $(dp)_{max}$ = 343.2 kPa, $(dS_w)_{max} = 0.2$, and $(dT)_{max} = 7.5$°C, to monitor pressure updates as well as to control convergence for solving Eq. (1). This run is named Base-Case.

5. 2. Examples of 2D Problem

First we performed a simulation of hot water-flooding in a 2D heterogeneous reservoir to evaluate the effects of the number of streamlines, the grid refinement on streamlines, and the time step size. A grid system of $15 \times 15 \times 1$ was employed. **Figure 2** shows the permeability field generated by the moving window method assuming the permeability has natural logarithm distribution with mean of −27.631 (0.9869×10^{-12} m^2, or 1000 md) and standard deviation of 0.5. The values range from 0.2773×10^{-12} m^2 (281 md) to 3.7354×10^{-12} m^2 (3785 md) as depicted by blue to red colors. The pressure and water saturation distributions shown in **Figs. 3(a)** and **(b)**, respectively, were attained by cold water-flooding, and were used as the starting conditions for hot water-flooding. The temperature distribution is nearly uniform at 52°C.

Comparisons of oil production rate, water cut, and oil recovery calculated from this thermal simulator by streamline (TESIS) and STARS are depicted in **Fig. 4**. The STARS solutions of oil rate and water cut are shown as smooth curves, whereas the TESIS solutions are shown as ragged curves, especially after 200 days. The agreements between both numerical methods are considered satisfactory, especially before 200 days. The departure appears after 200 days when breakthrough of the hot water of about 100°C has occurred. The lower oil rates of TESIS were most likely a result of the significant contribution of viscosity forces. As illustrated in **Fig. 5** for the viscosity and density of heavy oil used in this study, the viscosity decreases dramatically with a rise in temperature but the density changes are relatively less. In the sequential method, the new streamlines were obtained using the temperatures at the start of time step, which made the streamline velocity lower. Consequently, the new rate of heat flow was insufficient to attain the high temperature breakthrough. This is a known problem associated with the streamline methods based on an IMPES sequential approach, which causes unstable behavior when the fluid properties are a strong function of pressure.

The sensitivity of the solution to the number of streamlines is also demonstrated in **Fig. 4**. **Figure 4(b)** indicates that the solution improve with increasing number of streamlines. All these streamline solutions were obtained with the irregularly spaced τ grid on the streamlines. The dashed line with square symbol (150 SL-RG) illustrates a solution with the regular τ grid

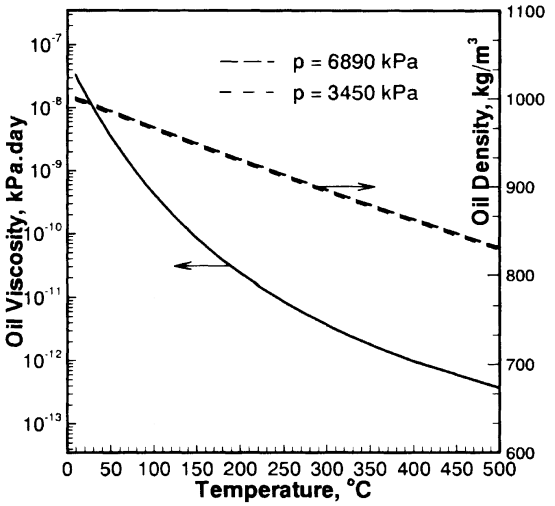

Fig. 5 Viscosity and Density of Heavy Oil Used for Simulation

using 150 streamlines. The number of nodes for the regularly spaced τ was determined as the number of the grid-blocks that a streamline passed through multiplied by two[9]. Transforming onto a regular τ grid tends to reduce the computing time of the simulation as confirmed by examples, but becomes a source of numerical diffusion in the streamline method[9] which would explain the obtained lower oil recovery among others in **Fig. 4(b)**. Analysis of the streamline number and the τ grid size was primarily done to confirm whether the simulation speed of this model could be improved.

Effects of hot water-flooding to improve recovery in a heavy oil reservoir can be observed in **Fig. 4(a)**. The onset of increased oil production coincides with the breakthrough of heated water to the producer at about 100 days. The water cut increases significantly in the early period, and then decreases again consistently with increase in the oil production.

Figures 6-8 present visual comparisons of the pressure, water saturation, and temperature distributions obtained by TESIS and STARS. These figures provide insight into the reasons for the similarities and differences depicted by the production performance curves in **Fig. 4**. The distortion of the fronts of water saturation and temperature was caused by the high heterogeneity of permeability. The presence of a more permeable region at the left top caused the growth of the front zone to deviate from predominant flow direction and veer to the left. This pattern appears to be similar in the results of both models.

Until 200 days, hot water injected nearly balanced total production, but the total production from the reservoir thereafter exceeded hot water injected by about 25%. This changed the streamline pattern (see **Figs. 9(a)**, **(b)**), and the need for re-mapping of temperature back to the grid after solving on the stream-

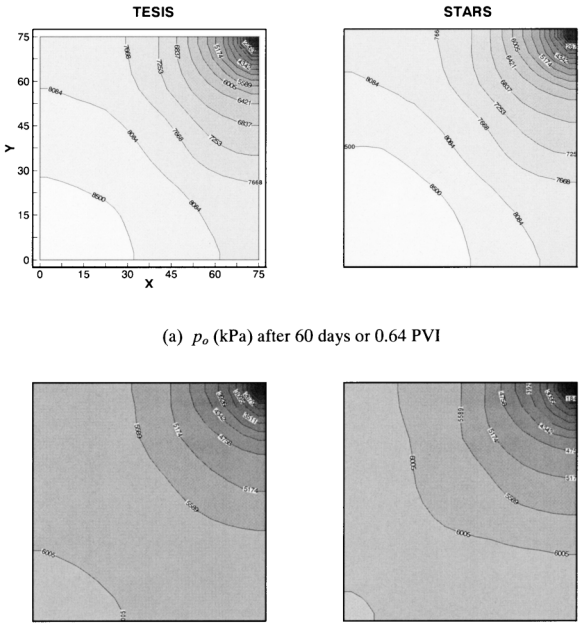

Fig. 6 Comparison of Pressure Distributions of 2D Simulation, (a) p_o (kPa) after 60 days or 0.64 PVI, (b) p_o (kPa) after 200 days or 2.12 PVI

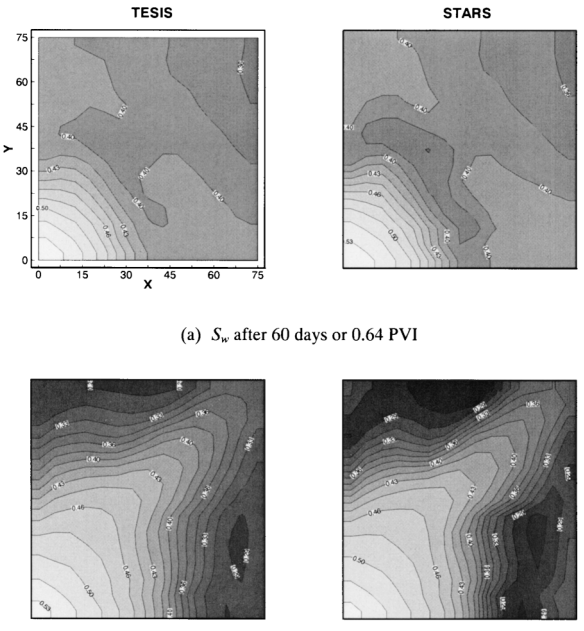

Fig. 7 Comparison of Water Saturation Distributions of 2D Simulation, (a) S_w after 60 days or 0.64 PVI, (b) S_w after 200 days or 2.12 PVI

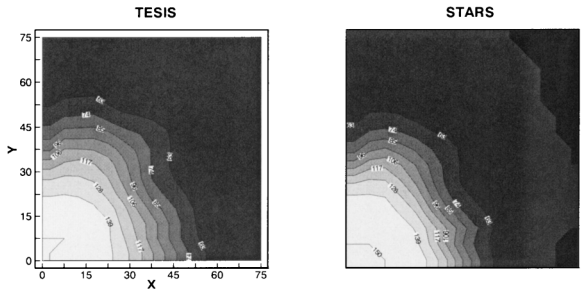

(a) T (°C) after 60 days or 0.64 PVI

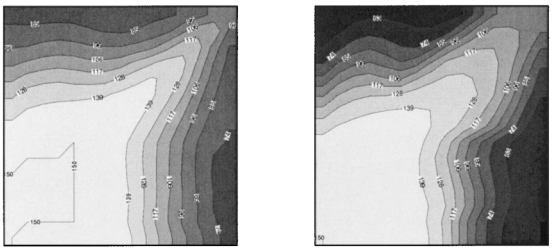

(b) T (°C) after 200 days or 2.12 PVI

Fig. 8 Comparison of Temperature Distributions of 2D Simulation, (a) T (°C) after 60 days or 0.64 PVI, (b) T (°C) after 200 days or 2.12 PVI

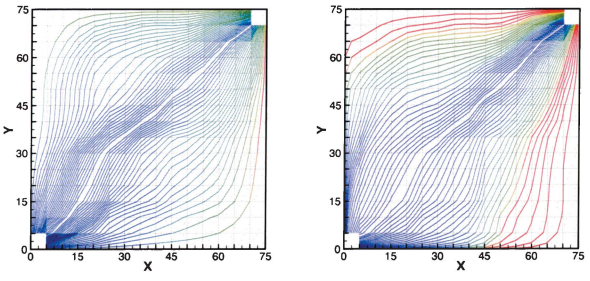

(a) Streamline Pattern at 100 days (b) Streamline Pattern at 200 days

Fig. 9 Streamline Patterns Colored by Time-of-flight, (a) Streamline Pattern at 100 days, (b) Streamline Pattern at 200 days

lines became apparent. As re-mapping back to the grid produces smears in the temperature solution, the material balance in general is not preserved exactly. This explains the higher total material balance error in TESIS rather than STARS shown in **Table 2**. **Figures 9(a)** and **(b)** show that the streamline pattern changed significantly between 100 and 200 days. It is important to note that although the streamline pattern is changed, it consistently reflects the permeability field of the reservoir.

There are a few missed grid-blocks in **Figs. 9(a)**, **(b)**. Missed grid-blocks typically have very low flow rates and thus very large τ's associated with them as shown by the red color at the edge corner regions in

Table 2 Comparison of Total Material Balance Error between TESIS and STARS

Time days	Total material balance error			
	TESIS 2D	STARS 2D	TESIS 3D	STARS 3D
60	1.94E-2	5.48E-5	2.02E-2	1.63E-3
100	2.89E-2	1.75E-5	3.11E-2	1.97E-3
200	5.24E-2	1.64E-4	6.56E-2	2.02E-3
225	5.43E-2	1.71E-4	6.76E-2	2.00E-3
250	5.55E-2	1.86E-4	6.90E-2	1.97E-3
275	5.61E-2	1.85E-4	7.05E-2	1.93E-3
300	5.69E-2	2.04E-4	7.11E-2	1.89E-3

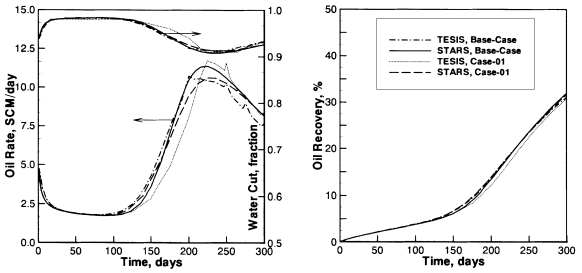

(a) Oil Rate and Water Cut (b) Oil Recovery

Fig. 10 Effects of Time Step Size on Production Behavior, (a) Oil Rate and Water Cut, (b) Oil Recovery

these figures.

Effects of the sequential time step for solving the mass balance and the energy balance equations are presented in **Fig. 10**. In this case, called Case-01, we ran TESIS and STARS using the numerical control (the maximum changes in the basic variables allowed over a time step) as $(dp)_{max} = 490.3$ kPa, $(dS_w)_{max} = 0.2$, and $(dT)_{max} = 25$°C. As these values except $(dS_w)_{max}$ were much larger than those for Base-Case, the time step size tended to be larger in Case-01 than in Base-Case. With a larger time step, the lower temperature of the previous time step is used for calculating mobility, and this causes still lower streamline velocity. As a result, the onset of incremental oil production is delayed, and the oil rate curve is shifted to the right leading to a larger difference between TESIS and STARS. In the STARS solution, pressure and temperature are solved implicitly, and completely aligned for each time step. The oil recovery for TESIS was also lower than for STARS. As expected, however, the total sequential iterations observed decreased significantly from 44 in Base-Case to 22 in Case-01.

5. 3. Examples of 3D Problem

We next ran the developed model with a 3D homogeneous reservoir of $75 \times 75 \times 5$ m^3 to examine how gravitational effects could be calculated. A grid system of $10 \times 10 \times 2$ was employed, and horizontal permeability of 1000 md and vertical permeability of 500 md were assigned to all grids. The initial pressure and

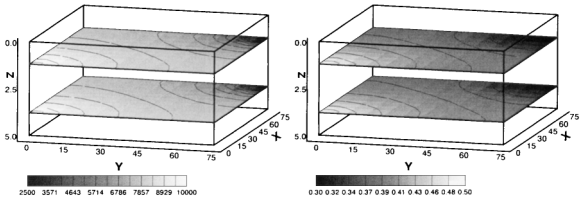

(a) Initial Oil Pressure (kPa) (b) Initial Water Saturation

Fig. 11 Initial Conditions of Pressure and Water Saturation for 3D Case, (a) Initial Oil Pressure (kPa), (b) Initial Water Saturation

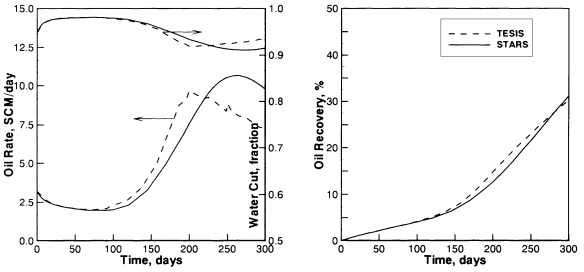

(a) Oil Rate and Water Cut (b) Oil Recovery

Fig. 12 Comparison of Production Performances of 3D Simulation, (a) Oil Rate and Water Cut, (b) Oil Recovery

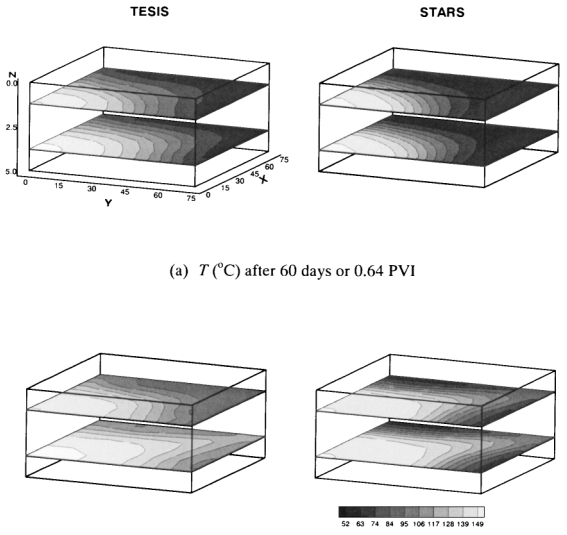

(a) T (°C) after 60 days or 0.64 PVI

(b) T (°C) after 200 days or 2.12 PVI

Fig. 13 Comparison of Temperature Distributions of 3D Simulation, (a) T (°C) after 60 days or 0.64 PVI, (b) T (°C) after 200 days or 2.12 PVI

water distributions are shown in **Figs. 11(a)** and **(b)**, respectively. Other data were identical to those used for the 2D simulation.

The production performance obtained by TESIS is

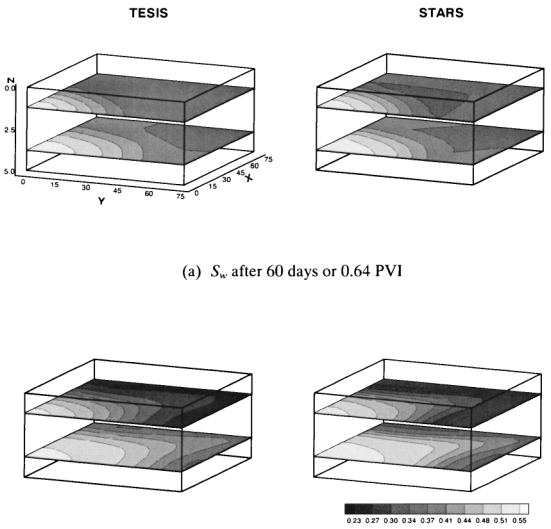

(a) S_w after 60 days or 0.64 PVI

(b) S_w after 200 days or 2.12 PVI

Fig. 14 Comparison of Water Saturation Distributions of 3D Simulation, (a) S_w after 60 days or 0.64 PVI, (b) S_w after 200 days or 2.12 PVI

shown in **Figs. 12(a)**, **(b)** together with the results of STARS. The major difference is the onset time of incremental oil production, about 100 days for TESIS against about 125 days for STARS. The difference is caused by the gravity under-ride occurring in this displacement process. TESIS modeled this gravity effect in more detail compared with STARS as shown in **Fig. 13**. A significant gravity tongue was developed in the lower layer (see **Fig. 13(b)**) which led to early breakthrough of the injected hot water and caused higher production. This is also the reason for the higher oil rates obtained by TESIS than by STARS between 100 and 200 days (see **Fig. 12(a)**). Comparisons of the water saturation and pressure profiles shown in **Figs. 14** and **15** also provide insight into the early increase of oil production. The final water saturation distribution in the upper layer remained low, particularly in regions with less contact with the injected fluid.

Streamlines also highlight how the fluids move through a reservoir depending on local conditions. **Figures 16(a)**, **(b)**, and **(c)** illustrate the streamlines of the water, oil, and total flows, respectively. The streamlines demonstrate how each phase flows. Water flows to the bottom of the reservoir in advance towards the production well due to gravity since it is heavier than oil, whereas oil flows from the bottom to the top of the reservoir. The total fluid flow demonstrates the tendency of the fluid to flow to the bottom resulting in high production rate from the second layer as discussed above. **Figures 16(a)** and **(b)** also indicate the strong contrast in flow velocity between the water and oil phases caused mainly by the differences

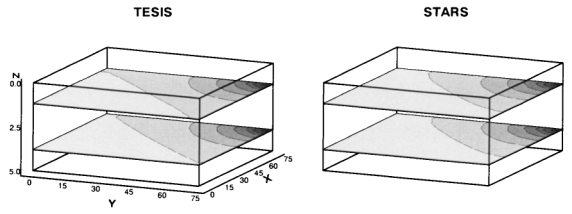

(a) p_o (kPa) after 60 days or 0.64 PVI

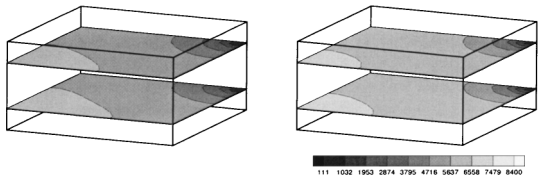

(b) p_o (kPa) after 200 days or 2.12 PVI

Fig. 15 Comparison of Pressure Distributions of 3D Simulation, (a) p_o (kPa) after 60 days or 0.64 PVI, (b) p_o (kPa) after 200 days or 2.12 PVI

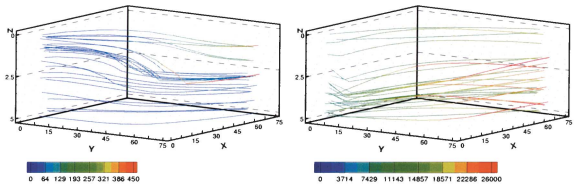

(a) Streamlines for Water Flow (b) Streamlines for Oil Flow

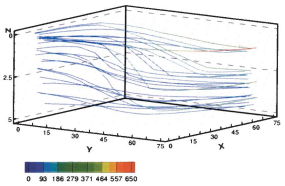

(c) Streamlines for Total Flow

Fig. 16 Streamline Patterns of Fluid Phases at 250 days, (a) Streamlines for Water Flow, (b) Streamlines for Oil Flow, (c) Streamlines for Total Flow

in viscosities. The maximum time-of-flight, τ, of all the water streamlines, calculated with the pressure field at 250 days, was estimated to be about 450 days for the travel between the injector and producer, whereas that of the oil phase was 26,000 days.

6. Conclusions

We derived a mathematical model for heat transport based on the streamline method. A numerical scheme using an operator splitting technique was applied to decouple the convection and the diffusions parts for separate solution. A thermal simulator utilizing sequential solutions of mass and heat flow equations was constructed to test this scheme. Simulations of hot water-flooding in 2D and 3D heavy-oil reservoirs were conducted to demonstrate the performance of the developed model.

The results of the 2D simulation compared well with the results of a commercial thermal simulator. Excellent agreements were obtained for the oil recovery performance. The solutions for the heat transport equation were obtained using the irregularly spaced τ grid not restricted by CFL conditions. The practical time step was 0.2 to 1.0 times the time step for the pressure solutions. In the 3D simulation, the streamline method demonstrated in more detail how the gravity under-ride mechanism affects the production performance. The test simulations demonstrated that the streamline approach could correctly model thermal transport and therefore is a viable alternative to conventional finite-difference models for the heat transport calculation within a thermal simulator. TESIS proved to be no faster than STARS due to inadequate LU decomposition of the matrix solver used in TESIS. However, there is potential for speedup. From the present examples, we found that TESIS required 43 time steps for the 2D model and 40 time steps for the 3D model compared to STARS that required 52 and 63 time steps, respectively. TESIS decoupled the mass and energy conservation equations as opposed to solving them simultaneously in STARS, which results in the smaller time step requirement.

Further work is to implement an appropriate rule of time-step selection for this numerical scheme, to develop an implicit streamline thermal simulator in which saturation and temperature are solved simultaneously along streamlines, and to improve the calculation time.

Acknowledgment

The first author wishes to thank Japan Oil, Gas and Metals National Corporation, INPEX Corporation, and Waseda University, School of Science and Engineering for the research assistantship.

Nomenclatures

A_x	: cross section x-direction	[m^2]
c_r	: rock compressibility	[Pa^{-1}]
C_r	: specific heat of rock	[kJ/(kg·°C)]
C_g	: specific heat of gas phase	[kJ/(kg·°C)]
D	: depth of gridblock from datum	[m]
f_α	: fractional flow of phase α	[fraction]

H_α : enthalpy of phase α [kJ/kg]
k : absolute permeability [m^2]
k_d : time step size for diffusion solution [day]
K_h : total thermal conductivity [kJ/(m·sec·°C)]
$k_{r\alpha}$: relative permeability of phase α [—]
N_d : number of time step for diffusion solution [—]
$\mathbf{n}$: unit vector outward normal to the boundary $\partial\Omega$ [—]
P_{cwo} : water-oil capillary pressure [Pa]
p_{ref} : reference pressure [Pa]
p_α : pressure of phase α [Pa]
q_α : source or sink flow rate per unit reservoir volume [kg/(day·m^3)]
s : local streamline coordinate [m]
S_α : saturation of phase α [fraction]
T : temperature [°C]
t : time [day]
$\mathbf{u}_\alpha$: Darcy velocity of phase α [m/day]
$\mathbf{x}$: Cartesian domain, (x, y, z) [—]

<Greeks>

Δt : time step size [day]
Δx : gridblock dimension in x-direction [m]
Δz : gridblock dimension in z-direction [m]
ζ : spatial distance coordinate along streamline [m]
λ_t : total mobility [(m^3·day)/kg]
λ_α : mobility of phase α [(m^3·day)/kg]
μ_α : viscosity of phase α [Pa·day]
Ω : reservoir domain [—]
ρ_r : rock density [kg/m^3]
ρ_α : density of phase α [kg/m^3]
τ : time-of-flight [day]
ϕ : porosity [fraction]
ϕ_{ref} : porosity at reference pressure [fraction]

<Subscripts>

c : convection
cr : critical
d : diffusion
g : gas
i, j, k : gridblock indices
inj : injection
o : oil
sc : surface conditions
t : total
vap : vapor
w : water

<Superscripts>

k, n : number of time step
o : initial conditions
v : number of Newton iterations
w : well

References

1) Doyle, R. E., Wurl, T. M., *Journal of Petroleum Technology*, **23**, 373 (1971).
2) Martin, J. C., Wegner, R. E., *SPE Journal*, **31**, 313 (1979).
3) Renard, G., *In Situ*, **14**, (2), 175 (1990).
4) Batycky, R. P., Thiele, M. R., Blunt, M. J., The 10th Annual Report, Stanford Center for Reservoir Forecasting (SCRF), Stanford University (1997).
5) Ponting, D. K., Proceedings of the SPE Asia Pacific Conference, Kuala Lumpur, Malaysia, 1998, Paper SPE 39756.
6) Ingebrigtsen, L., Bratvedt, F., Berge, J., Proceedings of the SPE Reservoir Simulation Symposium, Houston, Texas, 1999, Paper SPE 51904.
7) Crane, M., Bratvedt, F., Bratvedt, K., Childs, P., Olufsen, R., Proceedings of the SPE Annual Technical Conference and Exhibition, Dallas, Texas, 2000, Paper SPE 63156.
8) Bratvedt, F., Gimse, T., Tegnander, C., *Transport in Porous Media*, **25**, (1), 63 (1996).
9) Batycky, R. P., Thesis, Stanford University, California, USA, 1997.
10) Computer Modeling Group Ltd., STARS Version 2003 User's Guide, Calgary, Canada (2003).
11) Brantferger, K. M., Pope, G. A., Sepehrnoori, K., Proceedings of the 11th SPE Symposium on Reservoir Simulation, Anaheim, California, 1991, Paper SPE 21253.
12) Cicek, S., Ertekin, T., Proceedings of the European 3-D Reservoir Modeling Conference, Stavenger, Norway, 1996, Paper SPE 35516.
13) Peaceman, D. W., *SPE Journal*, **23**, (3), 531 (1983).
14) Shutler, N. D., Proceedings of the SPE 43rd Annual Fall Meeting, Houston, Texas, 1968, Paper SPE 2233.
15) Coats, K. H., *SPE Journal*, **28**, 235 (1976).
16) Pollock, D. W., *Ground. Water*, **26**, (6), 743 (1988).
17) Aziz, K., Settari, A., "Petroleum Reservoir Simulation," Applied Science Publisher, New York (1979).
18) Fanchi, J. R., "Integrated Flow Modeling," Elsevier Science B. V., Amsterdam (2000).
19) Datta-Gupta, A., King, M. J., *Advances in Water Resources*, **18**, 9 (1995).
20) Karlsen, K. H., Risebro, N. H., *Numer. Math.*, **77**, (3), 365 (1997).
21) Karlsen, K. H., Lie, K. A., Risebro, N. H., Frøyen, J., *In Situ*, **22**, (1), 59 (1998).
22) Karlsen, K. H., Lie, K. A., *IMA. J. Numer. Anal.*, **19**, (4), 609 (1999).

要　　旨

熱回収シミュレーションのためのストリームライン法による熱流動モデルの構築

ウスマン，在原　典男

早稲田大学大学院理工学研究科地球・環境資源理工学専攻，169-8555 東京都新宿区大久保3-4-1

本研究は，ストリームライン法を熱攻法による油回収のシミュレーションに拡張することを目指したものである。そのため，ストリームライン法に基づく熱流動モデルを構築し，熱攻法シミュレーターに組み込んだ。熱流動方程式は，流体流動による熱移流項と，重力，毛細管圧力，および伝導による熱拡散項から構成される。数値解法として，演算子分割により移流と拡散を分離する手法を適用した。熱移流は1次元非線形双曲線型方程式で表され，その解法にはストリームラインに沿って陰的単点風上（single-point upwind）スキームを適用した。熱拡散は非線形双曲線・放物線混合型方程式の形となり，3次元グリッド上の有限差分法により解いた。ストリームラインの計算に必要な圧力は，圧縮率および毛細管圧力を考慮した流体流動式に有限差分ニュートン法を適用することにより求めた。構築したモデルの検証のために，2次元および3次元油層における重質油に対する熱水攻法のシミュレーションを行った。商用の熱攻法シミュレーターの結果と比較することによって，熱攻法シミュレーターにおける熱流動計算のために，ストリームライン法が従来の有限差分法の代替として有効であることを確認した。